

Theory of optical responses in clean multi-band superconductors

Junyeong Ahn^{1,2,*} and Naoto Nagaosa^{2,3,†}

¹Department of Physics, Harvard University, Cambridge, Massachusetts 02138, USA

²RIKEN Center for Emergent Matter Science (CEMS), Wako, Saitama 351-0198, Japan

³Department of Applied Physics, The University of Tokyo, Bunkyo, Tokyo 113-8656, Japan
(Dated: March 15, 2021)

Electromagnetic responses in superconductors provide valuable information on the pairing symmetry as well as physical quantities such as the superfluid density. However, at the superconducting gap energy scale, optical excitations of the Bogoliubov quasiparticles are forbidden in conventional Bardeen-Cooper-Schrieffer superconductors when momentum is conserved. Accordingly, far-infrared optical responses have been understood in the framework of a dirty-limit theory by Mattis and Bardeen for over 60 years. Here we show, by investigating the selection rules imposed by particle-hole symmetry and unitary symmetries, that intrinsic momentum-conserving optical excitations can occur in clean multi-band superconductors when one of the following three conditions is satisfied: (i) inversion symmetry breaking, (ii) symmetry protection of the Bogoliubov Fermi surfaces, or (iii) simply finite spin-orbit coupling with unbroken time reversal and inversion symmetries. This result indicates that clean-limit optical responses are common beyond the straightforward case of broken inversion symmetry. We apply our theory to optical responses in FeSe, a clean multi-band superconductor with inversion symmetry and significant spin-orbit coupling. This result paves the way for studying clean-limit superconductors through optical measurements.

Introduction

Optical studies have been very important in superconductivity research since the superconducting gap was first observed by far-infrared optical measurements [1]. Not only does the optical absorption gap directly reveal the superconducting gap size, but also the loss of spectral weight of the optical conductivity in the superconducting transition shows the superfluid density [2–4]. Optical responses in superconductors are well understood by the dirty-limit theory of Mattis and Bardeen [5] and its extensions to arbitrary purity [6, 7]. Impurity is essential in the Mattis-Bardeen theory because Bogoliubov quasiparticles cannot be excited by uniform light when momentum is conserved in the Bardeen-Cooper-Schrieffer (BCS) model [8, 9]. In this paradigm, optical responses are due to impurity scattering and correspond to the Drude responses remaining in the superconducting state. They are thus completely described within a single-band model such as the BCS model and approaches the Drude formula as the photon energy increases above the gap [Fig. 1].

On the other hand, there have been cumulative studies revealing the relevance of multi-band effects in superconductivity. Strong gap anisotropy and multiple gap signatures due to orbital dependent pairing have been observed in various superconductors, including elemental metals Nb, Ta, V, and Pb [10, 11], compound MgB₂ [12], strontium titanates [13], iron pnictides and chalcogenides [14–16], and heavy fermion compounds [17, 18]. Multi-band effects are also considered to be important in the superconductivity of strontium ruthenates [19, 20], some half-Heusler compounds with $J = 3/2$ degrees of freedom [21–23], and twisted bilayer graphene [24–26]. This raises the question of whether multi-band effects can modify the optical responses. However, there has been no

observation of a significant deviation from the Mattis-Bardeen theory in any materials.

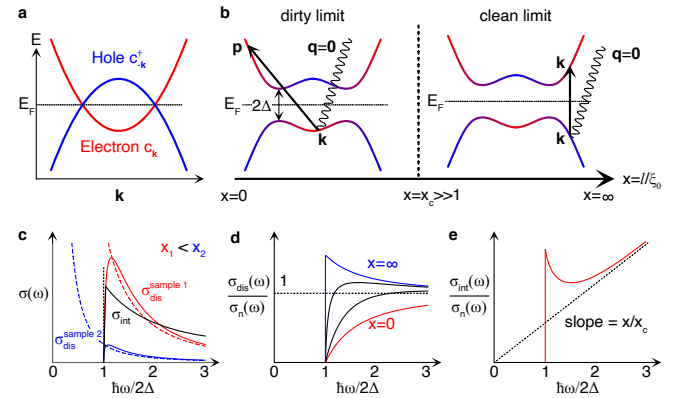


FIG. 1: Dirty and clean optical responses. **a**, Band structure in the Bogoliubov de-Gennes (BdG) formalism. Superconducting pairing opens the band gap at the Fermi level E_F by mixing electron (red) and hole (blue) bands as shown in **b**. c_k and c_{-k}^\dagger indicate the electron and hole annihilation operators, respectively. **b**, Optical excitations in dirty and clean limits by spatially uniform light ($\mathbf{q} = \mathbf{0}$) across the superconducting gap 2Δ . The momentum transfer $\mathbf{p} - \mathbf{k}$ in the left figure is supplied from the impurity potential. The crossover from dirty to clean optical responses occurs when the mean free path l exceeds the superconducting coherence length ξ_0 by a factor $x_c = (k_F \xi_0)^2 \alpha^{-2}$. Here, k_F is the Fermi wave number, and α is a degree of multi-band pairing (see the text above equation (6) for its more precise definition). The red and blue colors schematically represent the electron-hole band mixing in the superconducting state. **c**, Real part of the optical conductivity in clean systems ($x > 1$). $\sigma_s = \sigma_{\text{dis}} + \sigma_{\text{int}}$ in the superconducting state is the sum of disorder-mediated and intrinsic parts. $\sigma_{\text{int}} \propto \omega^{-1}$ is insensitive to x while $\sigma_{\text{dis}} \propto x^{-1} \omega^{-2}$ depends significantly on x . The Drude conductivity in the normal state σ_n is also shown as dashed lines. **d** and **e**, Ratio of superconducting and normal state conductivities. **d**, Disorder-mediated part. **e**, Intrinsic part.

* junyeongahn@fas.harvard.edu

† nagaosa@riken.jp

In this work, we challenge the Mattis-Bardeen paradigm by showing that a significant portion of the far-infrared optical response in a clean multi-band superconductor FeSe is due to intrinsic momentum-conserving excitations. We show that such intrinsic optical excitations are allowed by multi-band effects. To establish the criteria for non-zero intrinsic responses systematically, we present a tenfold way classification of optical excitations as well as selection rules due to unitary symmetries. Here, the tenfold way classification is by three symmetry operations \mathfrak{T} , \mathfrak{C} , and S that leave momentum invariant [27], whereas the original tenfold classification by Altland and Zirnbauer [28, 29] is by three spatially local symmetries, including time reversal T , particle-hole conjugation C , and chiral S symmetries [see Table 1]. Since T and C reverses the momentum, the combination of them with spatial inversion P (or any other momentum-reversing unitary operation) defines \mathfrak{T} and \mathfrak{C} . In this classification, \mathfrak{C} symmetry is the key player that imposes a new selection rule. We find that the absence of intrinsic optical excitations in single-band models can be attributed to \mathfrak{C} symmetry in the superconducting state.

As real materials are always accompanied by disorder, intrinsic responses coexist with disorder-mediated responses. A superconductor is considered to be clean when the mean free path l is larger than the superconducting coherence length ξ_0 and to be dirty when l is smaller than ξ_0 . We show that the crossover from disorder-mediated to intrinsic optical responses occurs at a very clean regime $l \sim (k_F \xi_0)^2 \alpha^{-2} \xi_0 \gg \xi_0$, as illustrated in Fig. 1(b), where k_F is the Fermi wave number, and $0 \leq \alpha \leq 1$ is a degree of multi-band pairing explained below. When l goes above this value, the optical conductivity follows the ω^{-1} behavior of the intrinsic response, deviating from the Drude-like ω^{-2} behavior [Fig. 1(d-e)]. We discuss the optical response of superconducting FeSe, which is closest to this crossover regime.

Results

Setting

Our theory is based on the mean-field theory of superconductors. We assume uniform illumination of light at zero temperature and the conservation of momentum. In momentum space, the single-particle mean-field Hamiltonian has the Bogoliubov-de Gennes (BdG) form

$$H(\mathbf{k}) = \begin{pmatrix} h(\mathbf{k}) & \Delta(\mathbf{k}) \\ -\Delta^*(-\mathbf{k}) & -h^T(-\mathbf{k}) \end{pmatrix} \quad (1)$$

in the basis of the Nambu spinor defined by $\hat{\psi} = (\hat{c}_{\rho s \mathbf{k}}, \hat{c}_{\rho s -\mathbf{k}}^\dagger)^T$, where $\hat{c}_{\rho s \mathbf{k}}$ is the electronic quasiparticle annihilation operator with orbital ρ and spin $s = \uparrow, \downarrow$ indices. Here, $h(\mathbf{k})$ is the normal-state Hamiltonian, and the pairing function $\Delta(\mathbf{k}) \propto \langle c_{\mathbf{k}} c_{-\mathbf{k}} \rangle$ satisfies $\Delta(\mathbf{k}) = -\Delta^T(-\mathbf{k})$ due to Fermi statistics of electrons. The BdG Hamiltonian always has particle-hole symmetry $CH(\mathbf{k})C^{-1} = -H(-\mathbf{k})$ under $C = \tau_x K$, where τ_x is a Pauli matrix for the particle-hole indices, and K is the complex conjugation operator.

The electromagnetic field couples to the normal-state Hamiltonian through the minimal coupling $\mathbf{k} \rightarrow \mathbf{k} + \frac{e}{\hbar} \mathbf{A}$, where $q = -e$ ($+e$) for the electron (hole) sector. It follows

that the velocity operator is

$$V^a(\mathbf{k}) = \frac{1}{e} \frac{\partial H}{\partial A_a} \Big|_{\mathbf{A}=0} = \frac{1}{\hbar} \begin{pmatrix} \partial_{k_a} h(\mathbf{k}) & 0 \\ 0 & \partial_{k_a} [h^T(-\mathbf{k})] \end{pmatrix}. \quad (2)$$

Matrix elements of this operator are important in our analysis because they describe the transition amplitudes. In the clean limit, the real part of the optical conductivity tensor is given by

$$\sigma^{ca}(\omega) = \frac{\pi e^2}{2\hbar\omega} \int_{\mathbf{k}} \sum_{n,m} f_{nm}(\mathbf{k}) V_{nm}^c(\mathbf{k}) V_{mn}^a(\mathbf{k}) \delta(\omega - \omega_{mn}(\mathbf{k})), \quad (3)$$

where ω is the frequency of light, $f_{nm} = f_n - f_m$ is the difference between the Fermi distribution of the n th band f_n , $V_{mn}^a = \langle m | V^a | n \rangle$, and $\omega_{mn} = \omega_m - \omega_n$, where $H|n\rangle = \hbar\omega_n|n\rangle$ [9, 30]. The delta function is replaced by the Lorentzian distribution when the mean free path is finite.

Selection rules

Equation (3) is positive-semidefinite when $c = a$. Therefore, inter-band transitions are completely forbidden only when symmetries impose $V_{mn}^a(\mathbf{k}) = 0$ at every \mathbf{k} [30]. The relevant symmetry operators should be \mathbf{k} -local ($\mathbf{k} \rightarrow \mathbf{k}$). A unitary symmetry imposes selection rules by $\lambda_m(\mathbf{k}) = \lambda_V(\mathbf{k})\lambda_n(\mathbf{k})$, where $\lambda_{m,n}$ and λ_V are symmetry eigenvalues of m, n states and the velocity operator, respectively. We always have $\lambda_V = 1$ because \mathbf{k} -local symmetry operations leave V^a invariant, as one might expect because the velocity operator should transform like \mathbf{k} . The selection rules thus simply becomes

$$V_{mn}^a(\mathbf{k}) = 0 \quad \text{when } \lambda_m(\mathbf{k}) \neq \lambda_n(\mathbf{k}), \quad (4)$$

meaning that optical excitations are forbidden between two different eigenspaces [Fig. 2(a)].

Let us consider the transition between two states in the same eigenspace of the unitary symmetry group. The remaining \mathbf{k} -local symmetries come in three types: anti-unitary \mathfrak{T} , anti-unitary anti-symmetry \mathfrak{C} , and unitary anti-symmetry S , where anti-symmetry means that the operator anti-commutes with the Hamiltonian. They form ten effective Altland-Zirnbauer (EAZ) symmetry classes [27–29, 31] shown in Table 1. \mathfrak{T} (or \mathfrak{C}) comes as a combination of T (or C) with a \mathbf{k} -reversing unitary operator such as spatial inversion P in any dimensions or twofold rotation C_{2z} in two dimensions. S is the combination $\mathfrak{T}\mathfrak{C}$ up to a phase factor. We find that only \mathfrak{C} -type symmetry can additionally exclude transition channels within an eigenspace of the unitary symmetry group. By using that \mathfrak{C} is anti-unitary and that the velocity operator is invariant under \mathfrak{C} , as shown in the Methods section 1, we have

$$\langle \mathfrak{C} \cdot n\mathbf{k} | V^a(\mathbf{k}) | n\mathbf{k} \rangle = 0 \quad \text{when } \mathfrak{C}^2 = -1. \quad (5)$$

This constrains, in particular, the lowest-energy excitations, as illustrated in Fig. 2(b,c). If bands are non-degenerate in each eigenspace, equation (5) indicates that the excitations across the gap are forbidden when $\mathfrak{C}^2 = -1$ [Fig. 2(b)]. See class C and CI in Table 1.

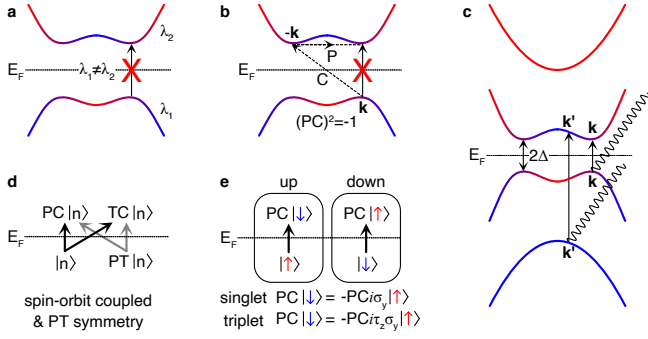


FIG. 2: Selection rules in clean superconductors. **a**, Selection rule by unitary symmetry. $\lambda_{1,2}$ are eigenvalues of a \mathbf{k} -local unitary symmetry operator. No optical excitation occurs between two states with different eigenvalues. **b**, Selection rule by \mathcal{C} symmetry. The case with $\mathcal{C} = PC$ is shown. No optical transition occurs between PC -related states when $(PC)^2 = -1$. **c**, Optical excitation channels in \mathcal{C} -symmetric superconductors in the clean limit. At low photon energies comparable to the superconducting gap 2Δ , the relevant excitations are spectrum-inversion-symmetric (SIS) ones, i.e., from energy $-E$ to E . For non-degenerate bands, they are transitions between \mathcal{C} -related pairs. **d** and **e**, Optical excitations in spin-degenerate systems with and without spin-orbit coupling, respectively. In **d**, $\mathfrak{T} = PT$ symmetry with $(PT)^2 = -1$ imposes Kramers degeneracy. As a state $|n\rangle$ can be excited to one of two SIS states, $PC|n\rangle$ and $PT(PC|n\rangle) = TC|n\rangle$, the excitation from $|n\rangle$ is possible even when one transition channel, from $|n\rangle$ to $PC|n\rangle$, is blocked by $(PC)^2 = -1$. The same applies to the excitation from $PT|n\rangle$. In **e**, the boxes labeled up and down indicate the spin up and down eigenspace ($s_z = \hbar/2$ and $-\hbar/2$, respectively). Since C reverses the spin (the anti-particle of a spin-up electron carries the down spin) while P does not change the spin, PC reverses the spin. Its combination with the spin rotation around the y axis, which is $i\sigma_y$ for spin-singlet pairing, acts within a s_z sector. For spin-triplet pairing, the spin rotation around the y axis acts on the particle and hole sector with an opposite sign due to the spin carried by the Cooper pair, so the additional τ_z is introduced (see section 3 in the Methods). Optical excitations are forbidden when \mathcal{C} defined within a spin sector, which is $-iPC\sigma_y$ for singlet pairing ($-iPC\tau_z\sigma_y$ for triplet pairing), satisfies $\mathcal{C}^2 = -1$. E_F is the Fermi level in all figures.

We find that the absence of optical excitations in single-band metal models, described by a two-band BdG Hamiltonian, can be attributed to the existence of $\mathcal{C} = i\tau_y K$ symmetry. A single-band metal has the \mathcal{C} symmetry in the superconducting state, independent of the pairing symmetry, when it has symmetry $\xi(\mathbf{k}) = \xi(-\mathbf{k})$ in the normal state, where $h(\mathbf{k}) = \xi(\mathbf{k})$ is the 1×1 Hamiltonian. Since the formation of Cooper pairs at the Fermi level requires such a symmetry relating \mathbf{k} and $-\mathbf{k}$, it means that typically no optical excitations can occur in superconductors originating from single-band metals. One can extend this result to show the absence of optical excitations in multi-band systems satisfying a generalized single-band pairing condition, the so-called the zero superconducting fitness condition (see section 2 in the Methods).

We have three ways of generating non-trivial optical excitations in an eigenspace. When bands are non-degenerate

within an eigenspace, one can (i) break \mathcal{C} symmetry (EAZ class A, AI, AII, and AIII) or (ii) realize $\mathcal{C}^2 = +1$ (class D and BDI). (iii) Or, when bands are Kramers degenerate due to \mathfrak{T} symmetry satisfying $\mathfrak{T}^2 = -1$, lowest-energy excitations are generally allowed irrespective of the sign of \mathcal{C}^2 (class DIII and CII). The first condition (i) just means breaking inversion symmetry when other unitary symmetries do not exist, which was demonstrated in Ref. [30]. The second (ii) implies that the superconductor may host stable Bogoliubov Fermi surfaces [27, 32]. Since $\mathcal{C}^2 = +1$ protects 0D \mathbb{Z}_2 topological charges, \mathbb{Z}_2 -stable nodal surfaces/lines/points in 3D/2D/1D can appear after superconducting pairing on the Fermi surfaces, respectively, which we call as Bogoliubov Fermi surfaces without distinguishing their dimension. Let us note that these are two-fold degenerate Bogoliubov Fermi surfaces. On the other hand, a stable non-degenerate Bogoliubov Fermi surface can appear in the EAZ classes A, AI, and AII. For instance, a superconductor with broken inversion and time reversal symmetries can host stable Bogoliubov Fermi surfaces [33–36]. Their stability is guaranteed by the change of the number of occupied BdG bands across the Bogoliubov Fermi surface, which is a \mathbb{Z} topological charge. Since these classes correspond to the case (i), the symmetry protection of the stable Bogoliubov Fermi surfaces, whether it is two-fold degenerate or not, indicates that the lowest-energy optical excitations are possible. The last possibility (iii) is realized in T - and P -symmetric systems with spin-orbit coupling. Because of the twofold band degeneracy imposed by $\mathfrak{T} = PT$ symmetry, there are two excitation channels

EAZ class	\mathfrak{T}^2	\mathcal{C}^2	S^2	Lowest excitation	BFS stability
A	0	0	0	Yes*	\mathbb{Z}
AI	1	0	0	Yes*	\mathbb{Z}
AII	-1	0	0	Yes*	\mathbb{Z}
AIII	0	0	1	Yes	0
D	0	1	0	Yes	\mathbb{Z}_2
BDI	1	1	1	Yes	\mathbb{Z}_2
C	0	-1	0	No	0
CI	1	-1	1	No	0
DIII	-1	1	1	Yes	0
CII	-1	-1	1	Yes	0

TABLE 1: Tenfold way classification of the lowest optical excitations in superconductors. Anti-unitary \mathfrak{T} , anti-unitary anti-symmetry \mathcal{C} , and unitary anti-symmetry S operators that do not change the momentum define ten effective Altland-Zirnbauer (EAZ) symmetry classes at a given generic momentum. 0 in the second set of columns indicates that no corresponding symmetry exists within the eigenspace of interest. When both \mathfrak{T} and \mathcal{C} symmetries exist, $S = \mathfrak{T}\mathcal{C}$ in classes BDI and CII ($S = i\mathfrak{T}\mathcal{C}$ in classes CI and DIII) when we choose the convention $\mathfrak{T}\mathcal{C} = \mathcal{C}\mathfrak{T}$. In classes A, AI, and AII, the lowest possible excitation energy within an eigenspace may not correspond to the direct superconducting gap, because the states with the lowest positive and the highest negative energies may have different symmetry eigenvalues. The asterisk (*) in the third column means that the excitation cannot occur when there is only one band in an eigenspace. The last column shows the stability of Bogoliubov Fermi surfaces (BFSs), meaning nodal surface/line/point in 3D/2D/1D superconductors.

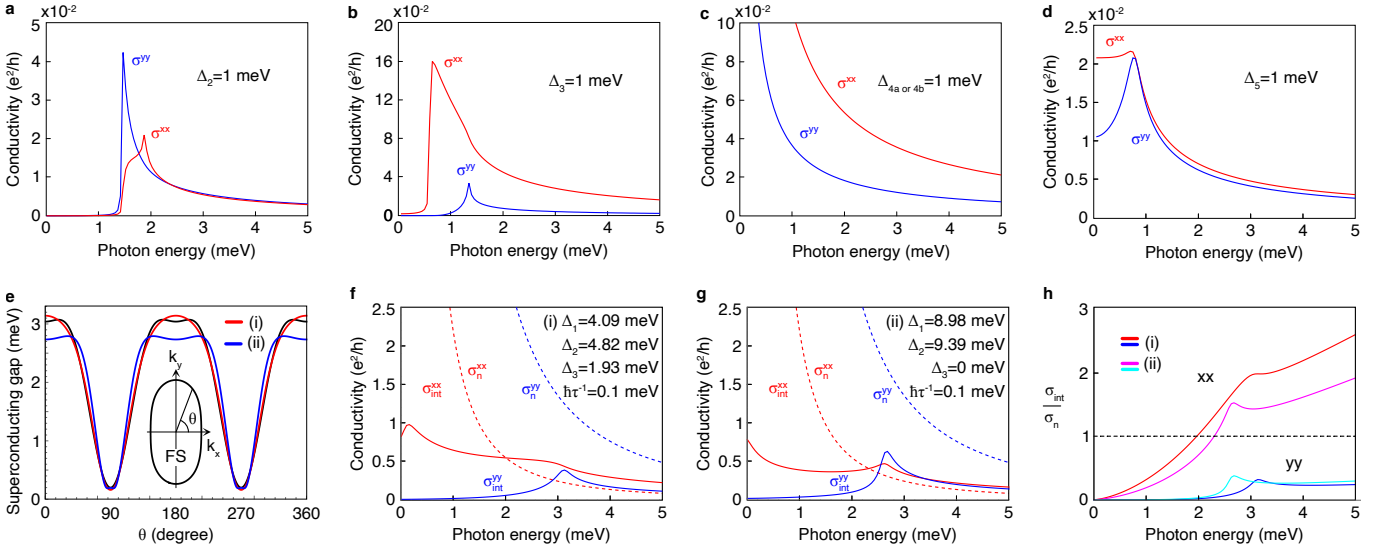


FIG. 3: Optical conductivity in a model of superconducting FeSe near Γ at zero temperature. Model parameters in the normal state are adopted from Ref. [39] (see section 6 in the Methods). The xx and yy components of the conductivity tensor is shown in red and blue, respectively, in **a** to **d**, **f**, and **g**. **a** to **d**, Non-zero intrinsic optical conductivity tensors for each constant pairing function. See Methods and Table 2 for the matrix form and symmetries of the six constant pairing functions Δ_1 , Δ_2 , Δ_3 , Δ_{4a} , Δ_{4b} , and Δ_5 . The case of the Δ_1 pairing is not shown as the conductivity is identically zero. **e**, Superconducting gap similar to the experimentally observed gap. FS and the ellipse enclosing it represent the Fermi surface. Red and blue curves correspond to the choice of pairing functions (i) $\Delta_1 = 4.09$ meV, $\Delta_2 = 4.82$ meV, and $\Delta_3 = 1.93$ meV or (ii) $\Delta_1 = 8.98$ meV, $\Delta_2 = 9.39$ meV, and $\Delta_3 = 0$ meV, respectively. They are least-square fits with and without Δ_3 to $\Delta(\theta) = |2.06 + 1.42 \cos(2\theta) - 0.44 \cos(4\theta)|$ (shown as a black curve) that was obtained in [15] from experimental data. **f** and **g**, Conductivity with pairing functions used in **e**. σ_{int} is the internal optical conductivity in the superconducting state (solid lines), and σ_n is the Drude conductivity in the normal state (dashed lines). The disorder-mediated conductivity in the superconducting state is expected to be comparable to σ_n . **h**, Ratio of σ_{int} and σ_n . Red and blue curves are for parameters in **f**, and magenta and cyan are for parameters in **g**. xx and yy indicate the component of the conductivity tensor. σ^{xy} and σ^{yx} are not shown in all plots because they vanish due to M_x symmetry.

where $|n\rangle$ at energy $-|E|$ can be excited to $+|E|$ as shown in Fig. 2(d). Even when one channel from $|n\rangle$ to $PC|n\rangle$ is excluded by $(PC)^2 = -1$, there exists another channel from $|n\rangle$ to $PT(PC|n\rangle) = TC|n\rangle$. In the absence of spin-orbit coupling, each spin sector forms non-degenerate states so that conditions (i) and (ii) apply [see Fig. 2(e) and section 3 in the Methods].

Crossover to clean-limit optical responses

In real materials, disorder is present even in very clean samples. We thus need to compare the magnitude of the disorder-mediated and intrinsic responses to characterize the detectability of the latter. We estimate the magnitude of the intrinsic response by counting the dimension of the conductivity tensor in equation (3), which gives $\sigma_{\text{int}}(\omega) \simeq \frac{e^2}{h} \frac{1}{\hbar\omega} \frac{(2\Delta)^2}{E_F} k_F^{d-2} \alpha^2$ above the gap, where k_F and E_F are the Fermi wave number and Fermi energy. Here, $0 \leq \alpha \leq 1$ is the ratio between the dominant pairing Δ and the pairing that are responsible for the optical conductivity. Comparing this with the disorder-mediated response, we obtain

$$\frac{\sigma_{\text{int}}(\omega)}{\sigma_{\text{dis}}(\omega)} \simeq \frac{\omega}{2\Delta} \frac{l}{\xi_0} \left(\frac{2\Delta}{E_F} \right)^2 \alpha^2 \quad (6)$$

above the superconducting gap, where we use that $\sigma_{\text{dis}}(\omega) \simeq \sigma_n(\omega)$ [5, 7] as shown in Fig. 1(d), where σ_n is the Drude conductivity in the normal state (see section 5 in the Methods).

We thus find that $\sigma_{\text{int}} \gtrsim \sigma_{\text{dis}}$ at $\hbar\omega \sim 2\Delta$ when

$$x \equiv l/\xi_0 > x_c = (k_F \xi_0)^2 \alpha^{-2}. \quad (7)$$

Since $x_c \gg 1$ in general because $k_F \xi_0 \sim E_F/\Delta \gg 1$ (E_F/Δ is about 10^4 for pure metals and 10^2 for most unconventional superconductors), the clean limit for optical responses is realized in samples much cleaner than that are usually thought to be clean, just satisfying $x > 1$. This explains how the Mattis-Bardeen-type theories have successfully calculated optical conductivity even in clean superconductors.

Application to FeSe

In FeSe, however, intrinsic optical responses can make up a significant portion of the observed signal in far-infrared optical measurements. FeSe is a clean quasi-two-dimensional material that has a remarkably large ratio $\Delta/E_F \gtrsim 0.1$ [37] with significant spin-orbit coupling comparable to the Fermi energy [38] and strongly orbital-dependent pairing [14], such that $\alpha \sim 1$ is expected. It therefore satisfies all the requirements for significant intrinsic optical responses. Here, we use the low-energy model of FeSe in Ref. [39] to demonstrate our theory, focusing on the Fermi surface near $\Gamma = (0, 0)$ for simplicity (see section 6 in the Methods).

We consider six constant pairing functions Δ_1 , Δ_2 , Δ_3 , Δ_{4a} , Δ_{4b} , and Δ_5 that preserve time reversal symmetry

Δ	Matrix	m_x	m_y	m_z	c_{4z}	Node	Lowest excitation
$\tilde{\Delta}_1$	$i\sigma_y$	+	+	+	+	Gapped	No
$\tilde{\Delta}_2$	$\rho_z i\sigma_y$	+	+	+	-	Gapped	Yes
$\tilde{\Delta}_3$	$\rho_y \sigma_z i\sigma_y$	+	+	+	+	Gapped	Yes
$\tilde{\Delta}_{4a}$	$\rho_y \sigma_x i\sigma_y$	-	+	-	$\tilde{\Delta}_{4b}$	Line	Yes
$\tilde{\Delta}_{4b}$	$\rho_y \sigma_y i\sigma_y$	+	-	-	$-\tilde{\Delta}_{4a}$	Line	Yes
$\tilde{\Delta}_5$	$\rho_x i\sigma_y$	-	-	+	-	Point	Yes

TABLE 2: Properties of time-reversal-symmetric constant pairing functions in a 2D model of FeSe at Γ . Here, $\tilde{\Delta}_1 = \Delta_1 i\sigma_y$, $\tilde{\Delta}_2 = \Delta_2 \rho_z i\sigma_y$, $\tilde{\Delta}_3 = \Delta_3 \rho_y \sigma_z i\sigma_y$, $\tilde{\Delta}_{4a} = \Delta_{4a} \rho_y \sigma_x i\sigma_y$, $\tilde{\Delta}_{4b} = \Delta_{4b} \rho_y \sigma_y i\sigma_y$, and $\tilde{\Delta}_5 = \Delta_5 \rho_x i\sigma_y$. The second column shows the result of transformation $u_g \Delta u_g^\dagger$ by $g = m_x, m_y, m_z$ or c_{4z} . The signs + and - means $+\Delta$ and $-\Delta$, respectively.

whose matrix forms and symmetries are given in the Methods and Table 2. All of them have even parity, but spin-triplet pairing can occur due to their multi-orbital nature (Δ_3 and $\Delta_{4a,4b}$). As we show in the Methods section 7, for even parity pairing, optical transitions are not forbidden within each M_z eigenspace in spin-orbit coupled systems. For $\Delta_{i=1,2,3,5}$ pairing, \mathcal{C} symmetry does not exist within a mirror sector. On the other hand, for $\Delta_{i=4a,4b}$, \mathcal{C} symmetry exists but satisfies $\mathcal{C}^2 = 1$ in each mirror sector. In accordance with our analysis, all multi-band pairing $\Delta_{i=2,3,4a,4b,5}$ allow for non-zero optical responses [Fig. 3(a-d)]. In the case of $\Delta_{i=4a,4b}$ and Δ_5 pairing, optical conductivity tensors are non-zero down to zero frequency because of their gapless spectrum due to the Bogoliubov Fermi surface and Dirac points, respectively [Fig. 3(d,e)].

In experiments, a highly anisotropic pairing gap was observed [14, 15], having a sinusoidal shape with $2 \sim 3$ meV peak at $k_y = 0$ and almost zero deep at $k_x = 0$. Supposing that the gap function belongs to the trivial representation of the symmetry group, we can obtain a similar anisotropic gap with a various combination of Δ_1 , Δ_2 , and Δ_3 . For example, we obtain (i) $\Delta_1 = 4.09$ meV, $\Delta_2 = 4.82$ meV, and $\Delta_3 = 1.93$ meV and (ii) $\Delta_1 = 8.98$ meV, $\Delta_2 = 9.39$ meV, and $\Delta_3 = 0$ meV, respectively, by least-square-fitting with and without spin-orbit coupled pairing Δ_3 to the function $\Delta(\theta) = |2.06 + 1.42 \cos(2\theta) - 0.44 \cos(4\theta)|$ derived from experimental data [15]. See Fig. 3(e). Despite the huge difference in pairing functions for (i) and (ii), the obtained conductivity is quite similar, as shown in Fig. 3(f-h). When $\hbar\tau^{-1} = 0.1$ meV ($l/\xi_0 \sim 10^2$), the xx component of the intrinsic optical conductivity in the superconducting state σ_{int}^{xx} exceeds the Drude conductivity in the normal state σ_n^{xx} at around $\hbar\omega \sim 2$ meV in both cases. Since the disorder-mediated response in the superconducting state is comparable to the normal-state response σ_n , the intrinsic response dominates above $\hbar\omega \sim 2$ meV along the x direction.

Discussion

Our theory establishes the existence of the true clean-limit optical responses beyond the Mattis-Bardeen theory in multi-band superconductors. While we focus on linear responses in the current work, our classification of optical transitions applies to nonlinear optical responses also [30].

Since nonlinear optical conductivity tensors have more components than the linear counterpart, they give richer information on the symmetry of the system. For instance, it is hard to detect inversion symmetry breaking from linear optical responses. On the other hand, since second-order optical responses are allowed only when inversion symmetry is broken, they directly reveal the presence of inversion symmetry [30]. As such, various optical measurements can be used in the study of clean multi-band superconductors. We anticipate an immediate impact of our work on the optical study of the exotic superconductivity in FeSe. Furthermore, our theory may be relevant to the recently discovered 2D superconductivities reaching $\Delta/E_F > 0.1$ in twisted trilayer graphene [40, 41] and ZrNCl [42]. As the synthesis of extremely clean superconductors advances further, our results will become relevant to more materials.

Methods

1. Selection rule by \mathcal{C} symmetry. Equation (5) can be simply derived as follows.

$$\begin{aligned}
\langle \mathcal{C} \cdot n\mathbf{k} | V^a(\mathbf{k}) n\mathbf{k} \rangle &= \langle \mathcal{C} V^a(\mathbf{k}) \cdot n\mathbf{k} | \mathcal{C}^2 \cdot n\mathbf{k} \rangle \\
&= \mathcal{C}^2 \langle \mathcal{C} \cdot n\mathbf{k} | \mathcal{C} V^a(\mathbf{k}) \mathcal{C}^{-1} | n\mathbf{k} \rangle \\
&= \epsilon_{\mathcal{C},V} \mathcal{C}^2 \langle \mathcal{C} \cdot n\mathbf{k} | V^a(\mathbf{k}) | n\mathbf{k} \rangle. \quad (8)
\end{aligned}$$

We use that \mathcal{C} is a anti-unitary operator in the first line, use that $\mathcal{C}^2 = \pm 1$ is a number, and V^a is Hermitian in the second line, and define $\epsilon_{\mathcal{C},V} = \pm 1$ by $\mathcal{C} V^a(\mathbf{k}) \mathcal{C}^{-1} = \epsilon_{\mathcal{C},V} V^a(\mathbf{k})$ in the third line. Let us recall that $V^a(\mathbf{k}) = \tau_z \partial_{k_a} H(\mathbf{k})$ for a BdG Hamiltonian $H(\mathbf{k})$. \mathcal{C} anti-commutes with τ_z because C anti-commutes with τ_z while a physical unitary operator U_g that combine to define $\mathcal{C} = U_g C$ commutes with τ_z . Since the \mathcal{C} symmetry condition imposes $\mathcal{C} H(\mathbf{k}) \mathcal{C}^{-1} = -H(\mathbf{k})$, we obtain $\epsilon_{\mathcal{C},V} = 1$, i.e., \mathcal{C} commutes with $V^a(\mathbf{k})$. Equation (5) then follows.

We note that normal-state systems with an emergent \mathcal{C} symmetry follow a different selection rule because they satisfy $\epsilon_{\mathcal{C},v} = -1$. The difference comes from the fact that, in the normal state, all quasi-particles are electronic quasi-particles that couple to the gauge field with the equal charge $-e$ (i.e., the emergent \mathcal{C} does not reverse the gauge charge). In this case, the velocity operator is $v^a(\mathbf{k}) = \partial_{k_a} h(\mathbf{k})$, where h is the \mathcal{C} -symmetric normal-state Hamiltonian, so that $\mathcal{C} v^a(\mathbf{k}) \mathcal{C}^{-1} = \partial_{k_a} \mathcal{C} h(\mathbf{k}) \mathcal{C}^{-1} = -v^a(\mathbf{k})$. The selection rule is then $\langle \mathcal{C} \cdot n\mathbf{k} | v^a(\mathbf{k}) | n\mathbf{k} \rangle = 0$ when $\mathcal{C}^2 = +1$, which is opposite to the superconducting case.

2. Optical excitations with a single-band condition. Let us suppose that the normal state is described by a single band, i.e., $h(\mathbf{k}) = \xi(\mathbf{k})$ is a 1×1 matrix. We consider the normal state having time reversal symmetry or inversion symmetry (or other symmetries whose action is equivalent to them [43]) because only then pairing between two electrons $c_{\mathbf{k}}$ and $c_{-\mathbf{k}}$ effectively occurs at the Fermi level. Then, $\xi(\mathbf{k}) = \xi(-\mathbf{k})$ such that $V^a(\mathbf{k}) = \hbar^{-1} \partial_a \xi(\mathbf{k}) \tau_0$ has vanishing inter-band matrix components for all \mathbf{k} , where τ_0 is the 2×2 identity matrix with the particle-hole indices. It follows that superconductivity in a single-band metal cannot exhibit non-trivial op-

tical conductivity in the clean limit. The same is true when the band has spin degeneracy at every \mathbf{k} , because $h(\mathbf{k}) = \xi(\mathbf{k})\sigma_0$ is again proportional to the identity matrix such that the velocity operator is diagonal.

These constraints can be understood from the \mathfrak{C} symmetry. Let us note that no identity term appears in the BdG Hamiltonian because we consider $\xi(\mathbf{k}) = \xi(-\mathbf{k})$. Thus, general two-band BdG Hamiltonian takes the form $H = g_x\tau_x + g_y\tau_y + g_z\tau_z$. It always satisfies $\mathfrak{C}H(\mathbf{k})\mathfrak{C}^{-1} = -H(\mathbf{k})$ for $\mathfrak{C} = i\tau_y K$, which satisfies $\mathfrak{C}^2 = -1$. This symmetry blocks optical transitions by equation (5). Let us consider the case where bands are twofold degenerate due to $\mathfrak{T}^2 = -1$ symmetry of the BdG Hamiltonian, where σ_y is an effective-spin Pauli matrix. As we assume time reversal or inversion symmetry, we also have \mathfrak{C} and S symmetries. We consider two cases with $\mathfrak{C}^2 = 1$ and $\mathfrak{C}^2 = -1$ by taking $\{\mathfrak{T} = i\sigma_y K, \mathfrak{C} = \tau_x K, S = \tau_x\sigma_y\}$ and $\{\mathfrak{T} = i\tau_z\sigma_y K, \mathfrak{C} = i\tau_y K, S = \tau_x\sigma_y\}$, respectively, such that $H = \xi\tau_z\sigma_0 + \Delta_s\tau_y\sigma_y$, and $H = \xi\tau_z\sigma_0 + (\Delta_t \cdot \sigma_y i\sigma_y\tau_+ + h.c.)$, where $\tau_+ = (\tau_x + i\tau_y)/2$. Since these correspond to the spin-singlet and spin-triplet pairing, there is a continuous spin rotation symmetry around an axis, such that the spin around the axis is a good quantum number. Each spin sector is thus described by a two-band BdG Hamiltonian having a \mathfrak{C} symmetry $\mathfrak{C}^2 = -1$.

We can extend the above results to show that the lowest-energy excitations, from $-E$ to E , are forbidden when a multi-band system satisfies the zero superconducting fitness [20, 44] condition, i.e., $[h(\mathbf{k}), \Delta^*(-\mathbf{k})] = 0$, which always holds when $\Delta(\mathbf{k})$ or $h(\mathbf{k})$ is proportional to the identity matrix. After we take simultaneous eigenstates of $h(\mathbf{k})$ and $\Delta^*(-\mathbf{k})$, the BdG Hamiltonian decomposes into a set of 2×2 blocks (4×4 blocks, in the presence of spin degeneracy), each of which correspond to a single-band superconductivity. It follows that transitions between two states with energies $-E$ and E are forbidden.

Let us explain it in more detail. When the zero superconducting fitness condition is satisfied, one can take eigenstates $|\alpha\mathbf{k}\rangle$ that satisfy $h(\mathbf{k})|\alpha\mathbf{k}\rangle = \xi_\alpha(\mathbf{k})|\alpha\mathbf{k}\rangle$, $\Delta^*(-\mathbf{k})|\alpha\mathbf{k}\rangle = \Delta_\alpha^*(-\mathbf{k})|\alpha\mathbf{k}\rangle$. In this basis, the BdG Hamiltonian is diagonalized into blocks labeled by α :

$$H_\alpha(\mathbf{k}) = \begin{pmatrix} \xi_\alpha(\mathbf{k}) & \Delta_\alpha(\mathbf{k}) \\ -\Delta_\alpha^*(-\mathbf{k}) & -\xi_\alpha(-\mathbf{k}) \end{pmatrix} \quad (9)$$

where the basis states $(1\ 0)^T$ and $(0\ 1)^T$ correspond to $|\alpha\mathbf{k}\rangle$ and $|\alpha-\mathbf{k}\rangle^*$, respectively. We assume either time reversal symmetry or inversion symmetry of the normal states, such that $\xi_\alpha(\mathbf{k}) = \xi_\alpha(-\mathbf{k})$.

The energy eigenstates of the BdG Hamiltonian are then

$$\begin{aligned} |\alpha, +, \mathbf{k}\rangle &= \begin{pmatrix} \cos\theta_\alpha(\mathbf{k})|\alpha\mathbf{k}\rangle \\ \sin\theta_\alpha(\mathbf{k})|\alpha-\mathbf{k}\rangle^* \end{pmatrix}, \\ |\alpha, -, \mathbf{k}\rangle &= \begin{pmatrix} -\sin\theta_\alpha(\mathbf{k})|\alpha\mathbf{k}\rangle \\ \cos\theta_\alpha(\mathbf{k})|\alpha-\mathbf{k}\rangle^* \end{pmatrix}, \end{aligned} \quad (10)$$

where $\cos\theta_\alpha(\mathbf{k}) = \xi_\alpha(\mathbf{k})/E_{\alpha,+}(\mathbf{k})$, $\sin\theta_\alpha(\mathbf{k}) = \Delta_\alpha(\mathbf{k})/E_{\alpha,+}(\mathbf{k})$, and $E_{\alpha,\pm}(\mathbf{k}) = \pm\sqrt{\xi_\alpha^2(\mathbf{k}) + \Delta_\alpha^2(\mathbf{k})}$. We

have

$$\begin{aligned} \langle \alpha, +, \mathbf{k} | v^a | \beta, -, \mathbf{k} \rangle &= \cos\theta(\mathbf{k}) \sin\theta(\mathbf{k}) [v_{\alpha\beta}^a(\mathbf{k}) + v_{\beta\alpha}^a(-\mathbf{k})] \\ &= 0 \quad (\text{for } \alpha = \beta), \end{aligned} \quad (11)$$

where the normal-state velocity operator

$$v_{\alpha\beta}^a(\mathbf{k}) = \hbar^{-1} \langle \alpha\mathbf{k} | \partial_a h(\mathbf{k}) | \beta\mathbf{k} \rangle \quad (12)$$

satisfy $v_{\alpha\alpha}^a(\mathbf{k}) = -v_{\alpha\alpha}^a(-\mathbf{k})$ due to either time reversal or inversion symmetry. Thus, assuming non-degenerate states, we immediately see that all transitions from $E_{\alpha,-}(\mathbf{k})$ to $E_{\alpha,+}(\mathbf{k}) = -E_{\alpha,-}(\mathbf{k})$ are forbidden because of the vanishing velocity matrix elements.

The transition between two states with energies $-E$ and E is forbidden even when spin (or pseudo-spin in spin-orbit coupled systems) degeneracy exists. Spin degeneracy can be imposed either by PT symmetry or spin rotation symmetry. In either case, the normal-state velocity matrix element between two spin-degenerate states $|\alpha\mathbf{k}\rangle$ and $|\beta\mathbf{k}\rangle$ vanishes by symmetry, i.e., $v_{\alpha\beta}^a(\mathbf{k}) = 0$. Let us first consider the case where the degeneracy is due to PT symmetry satisfying $(PT)^2 = -1$. Then we have $v_{\alpha,\beta=PT\alpha}^a(\mathbf{k}) = -v_{\alpha,PT\alpha}^a(\mathbf{k})$. When spin rotation symmetry exists, the constraint

$$v_{\uparrow\downarrow}^a(\mathbf{k}) = 0 \quad (13)$$

simply follows from the spin-rotation invariance of the velocity operator. equation (11) then shows $\langle \alpha, +, \mathbf{k} | v^a | \beta, -, \mathbf{k} \rangle = 0$ for α and β related by either PT or a spin rotation. Combining this with $\langle \alpha, +, \mathbf{k} | v^a | \alpha, -, \mathbf{k} \rangle = 0$, we see that all transition channels from $E_{\alpha,-} = E_{\beta,-}$ to $-E_{\alpha,-} = -E_{\beta,-}$ are forbidden.

3. Optical excitations with spin rotation symmetries.

Let us consider the EAZ classes within spin sectors for example. We first assume that time reversal, spatial inversion, a spin $U(1)$ rotation, and a spin π rotation (around an axis perpendicular to the $U(1)$ axis) symmetries are all present. Let us take energy eigenstates such that they carry definite spin along the z direction. In the case of triplet pairing, this means that we take the z direction as the triplet spin direction, because continuous spin rotation symmetries around other directions are broken. Within each spin sector, bands are non-degenerate at generic momenta. As we show in Fig. 2(d), PC flips the spin because of particles-hole conjugation. However, the combination of spin π rotation, which is $-i\sigma_y$ for singlet pairing ($-i\tau_z\sigma_y$ for triplet pairing), and PC acts within a spin sector, so symmetry under this \mathfrak{C} -type operation constraints optical excitations through equation (5). Optical excitations between \mathfrak{C} -related pairs are allowed when $\mathfrak{C}^2 = (-i\sigma_y PC)^2 = -(PC)^2 = 1$ and $\mathfrak{C}^2 = (-i\tau_z\sigma_y PC)^2 = (PC)^2 = 1$, respectively, for singlet and triplet pairing, where Bogoliubov Fermi surfaces are stable. Since $(PC)^2 = +1$ (-1) for even- and odd-parity pairing (see section 4 in the Methods below), this requires exotic odd-parity singlet pairing or even-parity triplet pairing, which is possible only when multi-orbital pairing, e.g., an orbital triplet, is realized. Alternatively, if inversion symmetry

is broken or spin-orbit coupling is not negligible, optical excitations are allowed with fully gapped superconductivity. Let us note that s_z -preserving spin-orbit coupling is enough to allow optical excitations, because it breaks spin rotation symmetries around other axes such that $\mathcal{C} \propto i\sigma_y PC$ is broken in each spin sector. In general, spin-orbit coupling breaks all spin rotation symmetries, so two excitation channels are allowed [Fig. 2(e)].

4. Symmetry operator and pairing symmetry. Let u_g be a unitary operator that acts on space as $g : \mathbf{k} \rightarrow g\mathbf{k}$. Suppose that it is a symmetry operator of the normal state, i.e.,

$$u_g h(\mathbf{k}) u_g^{-1} = h(g\mathbf{k}), \quad (14)$$

and the pairing function has eigenvalues $e^{i\theta_g}$ under U_g , i.e.,

$$u_g \Delta(\mathbf{k}) u_g^T = e^{i\theta_g} \Delta(g\mathbf{k}). \quad (15)$$

Due to the non-trivial symmetry transformation of the pairing function, the BdG Hamiltonian is symmetric under

$$U_g = \begin{pmatrix} u_g & 0 \\ 0 & e^{i\theta_g} u_g^* \end{pmatrix}, \quad (16)$$

which rotates the hole sector by $e^{i\theta_g}$ more:

$$U_g H(\mathbf{k}) U_g^{-1} = H(g\mathbf{k}). \quad (17)$$

U_g satisfies the following commutation relation with the particle-hole conjugation operator C .

$$U_g C = e^{i\theta_g} C U_g. \quad (18)$$

Let us take two examples.

1. $U_g = P$ is spatial inversion: $e^{i\theta_g} = +1$ and -1 indicates even-parity and odd-parity pairing. Thus, $PC = +CP$ ($PC = -CP$) for even-parity (odd-parity) pairing.
2. U_g is a spin rotation around the y axis by π : $e^{i\theta_g} = +1$ always for a spin-singlet pairing, and $e^{i\theta_g} = -1$ when the pairing function is a spin triplet with its spin parallel (perpendicular) to the y axis.

5. Estimates of disorder-mediated and intrinsic responses in the clean regime. The disorder-mediated response in the superconducting state is comparable to the Drude response in the normal state. When the light frequency ω is much larger than the inverse relaxation time Γ , which is the case in the clean regime $\hbar\Gamma \ll \Delta \lesssim \hbar\omega$, the Drude conductivity is $\sigma_n(\omega) = \sigma_0 \frac{\Gamma^2}{\omega^2 + \Gamma^2} \approx \sigma_0 \frac{\Gamma^2}{\omega^2}$. Here, $\sigma_0 = \frac{ne^2\tau}{m} \approx \frac{e^2}{h} k_F^{d-2} (\hbar^{-1} E_F \tau)$ is the DC conductivity, where $m = \hbar^2 k_F^2 / (2E_F)$, and $n \sim k_F^d$. Since $\sigma_{\text{dis}} \sim \sigma_n$, we have

$$\sigma_{\text{dis}}(\omega) \sim \frac{e^2}{h} k_F^{d-2} \frac{E_F}{2\Delta} \left(\frac{\xi_0}{l} \right) \left(\frac{2\Delta}{\hbar\omega} \right)^2, \quad (19)$$

where we use $E_F \sim \hbar v_F k_F$, $\Delta \sim \hbar v_F \xi_0^{-1}$, and $l = v_F \Gamma^{-1}$.

To estimate the intrinsic response, let us note that the inter-band velocity operator is linear in the leading order of Δ' / E_F , where Δ' is the largest multi-band pairing that is allowed to generate inter-band transitions by the selection rules in equations (4) and (5). The conductivity tensor in equation (3) is thus proportional to Δ'^2 . Using that the delta function has the dimension ω^{-1} , and using the Fermi energy and wave number as other scales, we obtain

$$\sigma_{\text{int}}(\omega) \sim \frac{e^2}{h} \frac{1}{\hbar\omega} \frac{(2\Delta)^2}{E_F} k_F^{d-2} \alpha^2, \quad (20)$$

where $\alpha = |\Delta' / \Delta|$ is equal to or smaller than one since Δ is the dominant pairing strength by definition. It follows that

$$\frac{\sigma_{\text{int}}(\omega)}{\sigma_{\text{dis}}(\omega)} \sim \frac{\omega}{2\Delta} \frac{l}{\xi_0} \left(\frac{2\Delta}{E_F} \right)^2 \alpha^2. \quad (21)$$

above the superconducting gap frequency.

6. FeSe model at the Γ point. If we regard FeSe as a 2D system, it has three Fermi surfaces around $\Gamma = (0, 0)$, $X = (\pi, 0)$, and $Y = (0, \pi)$, respectively, in the 1-Fe Brillouin zone [16]. Here, we consider the Fermi surface near Γ . The Fermi surface of FeSe at Γ consists mainly of two orbital degrees of freedom d_{yz} and d_{xz} , so we take $\psi(\mathbf{k}) = (d_{yz}(\mathbf{k}), d_{xz}(\mathbf{k}))^T$ as the basis state. At zero temperature, the normal-state Hamiltonian has the form

$$h_\Gamma = h_0 + h_{\text{nem}} + h_{\text{SOC}}, \quad (22)$$

where $h_0 = \epsilon_\Gamma - A(k_x^2 + k_y^2) + B(k_x^2 - k_y^2)\rho_z - 2Ck_x k_y \rho_x$ is the most general spinless Hamiltonian in the tetragonal phase up to second order in \mathbf{k} , $h_{\text{nem}} = -D\rho_z$ is the constant part of the nematic terms that develops below $T_{\text{nem}} \sim 90$ K [45–47], and $h_{\text{SOC}} = \lambda\rho_y \sigma_z$ is the constant spin-orbit coupling. Here, $\rho_{i=x,y,z}$ and $\sigma_{i=x,y,z}$ are the Pauli matrices for orbital and spin degrees of freedom, respectively. h_0 and h_{SOC} have tetragonal D_{4h} symmetry under mirror $m_x = -i\rho_z \sigma_x$, $m_y = i\rho_z \sigma_y$, and $m_z = -i\sigma_z$, and fourfold rotation $c_{4z} = i\rho_y e^{-i\frac{\pi}{4}\sigma_z}$, while h_{nem} breaks c_{4z} symmetry down to c_{2z} symmetry. All have time reversal $t = i\sigma_y K$ symmetry. In our numerical calculations, we take parameters used in Ref. [39], which are $\epsilon_\Gamma = -9$ meV, $A = 700$ meV \AA^2 , $B = C = 484$ meV \AA^2 , $D = 15$ meV, and $\lambda = 10$ meV.

The bulk FeSe shows superconductivity below 8 K without a sign of time reversal symmetry breaking [16, 45]. We consider constant pairing functions invariant under time reversal. Since there are six 4×4 matrices that are invariant under $t = i\sigma_y K$, the pairing function has the form

$$\Delta(\mathbf{k}) = (\Delta_1 + \Delta_2 \rho_z + \Delta_3 \rho_y \sigma_z + \Delta_{4a} \rho_y \sigma_x + \Delta_{4b} \rho_y \sigma_y + \Delta_5 \rho_x) i\sigma_y, \quad (23)$$

where $\Delta_1, \Delta_2, \Delta_3, \Delta_{4a}, \Delta_{4b}$, and Δ_5 are all independent of \mathbf{k} . The pairing symmetry of each term under the D_{4h} point group is shown in Table 2. Let us note that all are even-parity pairing, i.e., invariant under $p = m_x m_y m_z = 1$. The orbital-singlet nature of Δ_3 and $\Delta_{4a,4b}$ allows them to be

spin triplet even though they have even parity.

7. Optical excitations in M_z , P , and T -symmetric 2D superconductors. In two-dimensional systems perpendicular to the z axis, M_z symmetry divides eigenstates into two distinct eigenspaces with M_z eigenvalues $\lambda = \pm i$. It imposes a selection rule.

Let $M_z C = \eta C M_z$, where $\eta = \pm 1$, and $M_z |n\rangle = \lambda_n |n\rangle$. Then, $M_z P C |n\rangle = \eta P C M_z |n\rangle = \eta P C \lambda_n |n\rangle = \eta \lambda_n^* P C |n\rangle = -\eta \lambda_n P C |n\rangle$. Thus, $|n\rangle$ and $P C |n\rangle$ has the different eigenvalues when $\eta = 1$ and has same eigenvalues when $\eta = -1$. In the former case, the optical transition from $|n\rangle$ to $P C |n\rangle$ is forbidden by M_z symmetry because they are in different eigenspaces (and the velocity operator does not

change the eigenspace), but the transition from $|n\rangle$ to $S|n\rangle$ is allowed. On the other hand, in the latter case, the transition from $|n\rangle$ to $P C |n\rangle$ within the same mirror sector is forbidden for when the pairing is odd-parity such that $(P C)^2 = -1$.

In summary, optical transitions between particle-hole- and chiral-related states are forbidden in P and T -symmetric systems when $M_z C = -C M_z$ and $P C = -C P$. Similar constraints can appear in one-dimensional systems also due to mirror symmetries.

Data Availability

The data that support the findings of this study are available from the corresponding author upon reasonable request.

-
- [1] Tinkham, M. Energy gap interpretation of experiments on infrared transmission through superconducting films. *Phys. Rev.* **104**, 845 (1956).
- [2] Tinkham, M. Far infrared absorption in superconductors. In *Far-Infrared Properties of Solids*, 223–246 (Springer, 1970).
- [3] Basov, D. & Timusk, T. Electrodynamics of high- T_c superconductors. *Rev. Mod. Phys.* **77**, 721 (2005).
- [4] Charnukha, A. Optical conductivity of iron-based superconductors. *J. Phys. Condens. Matter* **26**, 253203 (2014).
- [5] Mattis, D. & Bardeen, J. Theory of the anomalous skin effect in normal and superconducting metals. *Phys. Rev.* **111**, 412 (1958).
- [6] Leplae, L. Derivation of an expression for the conductivity of superconductors in terms of the normal-state conductivity. *Phys. Rev. B* **27**, 1911 (1983).
- [7] Zimmermann, W., Brandt, E., Bauer, M., Seider, E. & Genzel, L. Optical conductivity of bcs superconductors with arbitrary purity. *Physica C* **183**, 99–104 (1991).
- [8] Bardeen, J., Cooper, L. N. & Schrieffer, J. R. Theory of superconductivity. *Phys. Rev.* **108**, 1175 (1957).
- [9] Mahan, G. D. *Many-particle physics* (Springer Science & Business Media, 2013).
- [10] Shen, L. Y. L., Senozan, N. & Phillips, N. E. Evidence for two energy gaps in high-purity superconducting Nb, Ta, and V. *Phys. Rev. Lett.* **14**, 1025 (1965).
- [11] Blackford, B. & March, R. Tunneling investigation of energy-gap anisotropy in superconducting bulk Pb. *Phys. Rev.* **186**, 397 (1969).
- [12] Souma, S. *et al.* The origin of multiple superconducting gaps in MgB₂. *Nature* **423**, 65–67 (2003).
- [13] Binnig, G., Baratoff, A., Hoenig, H. & Bednorz, J. Two-band superconductivity in Nb-doped SrTiO₃. *Phys. Rev. Lett.* **45**, 1352 (1980).
- [14] Sprau, P. O. *et al.* Discovery of orbital-selective Cooper pairing in FeSe. *Science* **357**, 75–80 (2017).
- [15] Liu, D. *et al.* Orbital origin of extremely anisotropic superconducting gap in nematic phase of FeSe superconductor. *Phys. Rev. X* **8**, 031033 (2018).
- [16] Shibauchi, T., Hanaguri, T. & Matsuda, Y. Exotic superconducting states in FeSe-based materials. *J. Phys. Soc. Jpn* **89**, 102002 (2020).
- [17] Jourdan, M., Zakharov, A., Foerster, M. & Adrian, H. Evidence for multiband superconductivity in the heavy fermion compound UNi₂Al₃. *Phys. Rev. Lett.* **93**, 097001 (2004).
- [18] Mukuda, H. *et al.* Multiband superconductivity in heavy fermion compound CePt₃Si without inversion symmetry: An NMR study on a high-quality single crystal. *J. Phys. Soc. Jpn* **78**, 014705–014705 (2009).
- [19] Maeno, Y. *et al.* Superconductivity in a layered perovskite without copper. *Nature* **372**, 532–534 (1994).
- [20] Ramires, A. & Sigrist, M. Identifying detrimental effects for multiorbital superconductivity: Application to Sr₂RuO₄. *Phys. Rev. B* **94**, 104501 (2016).
- [21] Kim, H. *et al.* Beyond triplet: Unconventional superconductivity in a spin-3/2 topological semimetal. *Sci. Adv.* **4**, eaao4513 (2018).
- [22] Venderbos, J. W., Savary, L., Ruhman, J., Lee, P. A. & Fu, L. Pairing states of spin-3/2 fermions: Symmetry-enforced topological gap functions. *Phys. Rev. X* **8**, 011029 (2018).
- [23] Kawakami, T., Okamura, T., Kobayashi, S. & Sato, M. Topological crystalline materials of $j=3/2$ electrons: Antiperovskites, dirac points, and high winding topological superconductivity. *Phys. Rev. X* **8**, 041026 (2018).
- [24] Cao, Y. *et al.* Unconventional superconductivity in magic-angle graphene superlattices. *Nature* **556**, 43 (2018).
- [25] Po, H. C., Zou, L., Vishwanath, A. & Senthil, T. Origin of mott insulating behavior and superconductivity in twisted bilayer graphene. *Phys. Rev. X* **8**, 031089 (2018).
- [26] Xie, F., Song, Z., Lian, B. & Bernevig, B. A. Topology-bounded superfluid weight in twisted bilayer graphene. *Phys. Rev. Lett.* **124**, 167002 (2020).
- [27] Bzdušek, T. & Sigrist, M. Robust doubly charged nodal lines and nodal surfaces in centrosymmetric systems. *Phys. Rev. B* **96**, 155105 (2017).
- [28] Zirnbauer, M. R. Riemannian symmetric superspaces and their origin in random-matrix theory. *Journal of Mathematical Physics* **37**, 4986–5018 (1996).
- [29] Altland, A. & Zirnbauer, M. R. Nonstandard symmetry classes in mesoscopic normal-superconducting hybrid structures. *Phys. Rev. B* **55**, 1142 (1997).
- [30] Xu, T., Morimoto, T. & Moore, J. E. Nonlinear optical effects in inversion-symmetry-breaking superconductors. *Phys. Rev. B* **100**, 220501 (2019).
- [31] Shiozaki, K., Sato, M. & Gomi, K. Atiyah-hirzebruch spectral sequence in band topology: General formalism and topological invariants for 230 space groups. *Preprint at <http://arxiv.org/abs/1802.06694>* (2018).
- [32] Agterberg, D., Brydon, P. & Timm, C. Bogoliubov Fermi sur-

- faces in superconductors with broken time-reversal symmetry. *Phys. Rev. Lett.* **118**, 127001 (2017).
- [33] Volovik, G. Zeroes in the energy gap in superconductors with high transition temperature. *Physics Letters A* **142**, 282–284 (1989).
- [34] Berg, E., Chen, C.-C. & Kivelson, S. A. Stability of nodal quasiparticles in superconductors with coexisting orders. *Phys. Rev. Lett.* **100**, 027003 (2008).
- [35] Timm, C., Schnyder, A., Agterberg, D. & Brydon, P. Inflated nodes and surface states in superconducting half-Heusler compounds. *Phys. Rev. B* **96**, 094526 (2017).
- [36] Link, J. M. & Herbut, I. F. Bogoliubov-fermi surfaces in non-centrosymmetric multicomponent superconductors. *Phys. Rev. Lett.* **125**, 237004 (2020).
- [37] Terashima, T. *et al.* Anomalous Fermi surface in FeSe seen by Shubnikov–de Haas oscillation measurements. *Phys. Rev. B* **90**, 144517 (2014).
- [38] Borisenko, S. *et al.* Direct observation of spin–orbit coupling in iron-based superconductors. *Nat. Phys.* **12**, 311–317 (2016).
- [39] Udina, M., Grilli, M., Benfatto, L. & Chubukov, A. V. Raman response in the nematic phase of FeSe. *Phys. Rev. Lett.* **124**, 197602 (2020).
- [40] Park, J. M., Cao, Y., Watanabe, K., Taniguchi, T. & Jarillo-Herrero, P. Tunable phase boundaries and ultra-strong coupling superconductivity in mirror symmetric magic-angle trilayer graphene. *Preprint at <http://arxiv.org/abs/2012.01434>* (2020).
- [41] Hao, Z. *et al.* Electric field tunable unconventional superconductivity in alternating twist magic-angle trilayer graphene. *Preprint at <http://arxiv.org/abs/2012.02773>* (2020).
- [42] Nakagawa, Y. *et al.* Gate-controlled BCS-BEC crossover in a two-dimensional superconductor. *Preprint at <http://arxiv.org/abs/2012.05707>* (2020).
- [43] Fischer, M. H., Sigrist, M. & Agterberg, D. F. Superconductivity without inversion and time-reversal symmetries. *Phys. Rev. Lett.* **121**, 157003 (2018).
- [44] Ramirez, A., Agterberg, D. F. & Sigrist, M. Tailoring T_c by symmetry principles: The concept of superconducting fitness. *Phys. Rev. B* **98**, 024501 (2018).
- [45] Hsu, F.-C. *et al.* Superconductivity in the PbO-type structure α -FeSe. *Proc. Natl. Acad. Sci. U.S.A.* **105**, 14262–14264 (2008).
- [46] Margadonna, S. *et al.* Crystal structure of the new FeSe $_{1-x}$ superconductor. *ChemComm* 5607–5609 (2008).
- [47] McQueen, T. *et al.* Tetragonal-to-orthorhombic structural phase transition at 90 K in the superconductor Fe $_{1.01}$ Se. *Phys. Rev. Lett.* **103**, 057002 (2009).

Acknowledgements

We appreciate Takasada Shibauchi, Kenichiro Hashimoto, Yuta Mizukami, and Guang-Yu Guo for helpful discussions and thank Maine Christos for useful comments on the manuscript. J.A. was supported by the RIKEN Special Postdoctoral Researcher Program, the funding via Ashvin Vishwanath from the Center for Advancement of Topological Semimetals, an Energy Frontier Research Center funded by the US Department of Energy Office of Science, Office of Basic Energy Sciences, through the Ames Laboratory under contract No. DE-AC02-07CH11358, and Basic Science Research Program through the National Research Foundation of Korea (NRF) funded by the Ministry of Education (Grant No. 2020R1A6A3A03037129). N.N. was supported by JST CREST Grant Number JPMJCR1874 and JPMJCR16F1, Japan, and JSPS KAKENHI Grant Number 18H03676.

Author contributions

J.A. conceived the original idea and performed theoretical analysis. N.N. supervised the project and noticed the relevance of the theory to FeSe. Both authors discussed the data and wrote the manuscript.

Competing interests

The authors declare no competing interests.

Additional information

Correspondence and requests for materials should be addressed to J.A. or N.N.

Supplementary Note 1. Additional model calculations

We take two 2D models — respectively non-degenerate and twofold-degenerate at generic momenta — to further demonstrate our theory. The first is a model of single Dirac cone.

$$h_1 = -\mu + \hbar v k_x \sigma_y - \hbar v k_y \sigma_x, \quad (\text{S1})$$

where $\sigma_{i=x,y,z}$ is a spin Pauli matrix. It is symmetric under mirror $m_x = i\sigma_x$ and $m_y = i\sigma_y$, fourfold rotation $c_{4z} = e^{-i\pi\sigma_z/4}$, and time reversal $t = i\sigma_y K$. No mirror m_z and inversion p symmetries exist. Here, we use lowercase letters to denote symmetry operators of the normal state Hamiltonian to distinguish them from those of the BdG Hamiltonian. There are four possible superconducting pairing functions we list in Table. S1. When the pairing function is even (odd) under c_{2z} , the BdG Hamiltonian has symmetry under $\mathcal{C} = C_{2z}\mathcal{C}$ where $\mathcal{C}^2 = -1 (+1)$ because $C_{2z} = c_{2z} (C_{2z} = \tau_z c_{2z})$. In accordance with our general theory, conductivity tensors can be non-zero only when $\mathcal{C}^2 = 1$ if we keep \mathcal{C} symmetry [Fig. S1(a)]. In the limit $\omega, \Delta \ll \mu$, the non-zero conductivity can be analytically calculated as $\sigma^{cc} \sim \frac{e^2}{h} \frac{1}{\hbar\omega} \frac{(\Delta_4 k_F)^2}{E_F}$, where $E_F = \mu$ and $k_F = \mu/\hbar v$ (see Supplementary Note 2). $\sigma^{xy} = \sigma^{yx} = 0$ is due to mirror symmetries in our model. Figure S1(b) shows the case where \mathcal{C} symmetry is broken by a C_{2z} -parity mixing due to the additional s -wave pairing $\Delta_1 \neq 0$.

Next, we double the orbital degrees of freedom in equation (S1) and add a mass term to have a low-energy model of a doped 2D topological insulator.

$$h_2 = -\mu + \hbar v k_x \rho_x \sigma_y - \hbar v k_y \rho_x \sigma_x + M \rho_z, \quad (\text{S2})$$

where $\rho_{i=x,y,z}$ is an orbital Pauli matrix. It has $m_x = i\sigma_x$, $m_y = i\sigma_y$, $m_z = i\rho_z \sigma_z$, $c_{4z} = e^{-i\pi\sigma_z/4}$, and $t = i\sigma_y K$

$\Delta(\mathbf{k})$	m_x	m_y	c_{4z}	Node	Lowest excitation
$\Delta_1 i\sigma_y$	+	+	+	Gapped	No
$\Delta_2 (k_x \sigma_x + k_y \sigma_y) i\sigma_y$	-	-	+	Gapped	No
$\Delta_3 (k_x \sigma_x - k_y \sigma_y) i\sigma_y$	-	-	-	Point	No
$\Delta_{4a} k_x \sigma_z i\sigma_y$	-	+	$\begin{pmatrix} 0 & 1 \\ -1 & 0 \end{pmatrix}$	Line	Yes
$\Delta_{4b} k_y \sigma_z i\sigma_y$	+	-	$\begin{pmatrix} 0 & 1 \\ -1 & 0 \end{pmatrix}$	Line	Yes

TABLE S1: Time-reversal-symmetric pairing functions of a 2D single Dirac fermion model. Pairing functions are given up to the leading order in \mathbf{k} . The second column shows the matrix representation r_g defined by $u_g \Delta_i(\mathbf{k}) u_g^T = (r_g)_{ij} \Delta_j(g\mathbf{k})$.

$\Delta(\mathbf{k})$	m_x	m_y	m_z	c_{4z}	Node	Lowest excitation
$\Delta_1 i\sigma_y$	+	+	+	+	Gapped	No
$\Delta_2 \rho_z i\sigma_y$	+	+	+	+	Gapped	Yes
$\Delta_3 \rho_x i\sigma_y$	+	+	-	+	Gapped	No
$\Delta_4 \rho_y \sigma_z i\sigma_y$	-	-	-	+	Gapped	No
$\Delta_{5a} \rho_y \sigma_y i\sigma_y$	-	+	+	$\begin{pmatrix} 0 & -1 \\ 1 & 0 \end{pmatrix}$	Point	Yes
$\Delta_{5b} \rho_y \sigma_x i\sigma_y$	+	-	+	$\begin{pmatrix} 1 & 0 \\ 0 & 0 \end{pmatrix}$	Point	Yes

TABLE S2: Time-reversal-symmetric constant pairing functions of a 2D TI model. The second column shows the matrix representation r_g defined by $u_g \Delta_i(\mathbf{k}) u_g^T = (r_g)_{ij} \Delta_j(g\mathbf{k})$.

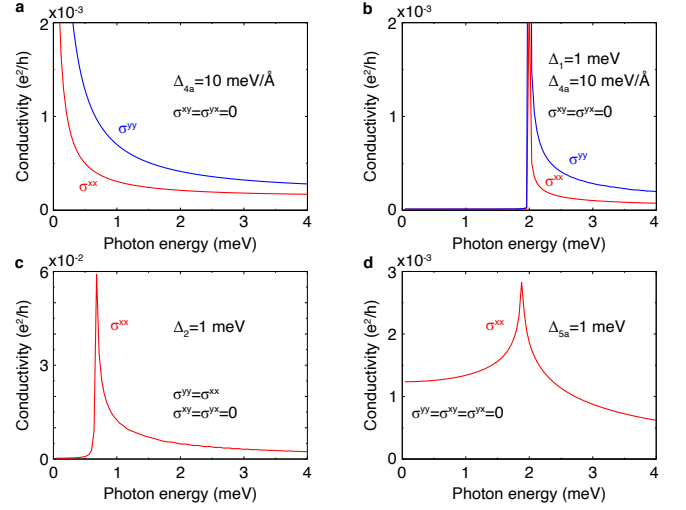


FIG. S1: Intrinsic optical conductivity in 2D superconductor models. **a, b**, Superconducting state of equation (S1) with $\mu = 0.1$ eV, $\hbar v = 1$ eV/Å, and the order parameters listed in Table. S1. **c, d**, Superconducting state of equation (S2) with $\mu = 0.15$ eV, $\hbar v = 1$ eV/Å, $M = 0.05$ eV, and the order parameters listed in Table. S2. As the spectrum is gapless in **a** and **d**, optical conductivity is non-zero down to zero frequency.

symmetries. $pt = i\rho_z \sigma_y K$ symmetry imposes Kramers degeneracy at each \mathbf{k} , where $p = m_x m_y m_z$. Since this model is spin-orbit coupled, optical excitations can generally occur, as illustrated in Fig. 2(d) of the main text. When the pairing is odd- m_z , however, optical excitations are not allowed because of the combination of the selection rules by unitary and PC symmetries (see Methods section 7 in the main text). Figure S1(c,d) shows non-zero optical conductivity tensors for constant pairing functions in Table S2. Let us note that, while Δ_2 has the same symmetry properties as the s -wave pairing under mirror operations and opens the full gap, we have non-zero optical conductivity without breaking any symmetry. In the case of Δ_5 pairing, the response is highly anisotropic, and, in fact, $\sigma^{yy} = 0$ while $\sigma^{xx} \neq 0$. The vanishing of σ^{yy} is not due to symmetry. It is a coincidence due to the fact that $\partial_y \hbar \propto \Delta$ (see Supplementary Note 3). We can generate $\sigma^{yy} \neq 0$, e.g., by adding quadratic terms in the mass term by $M \rightarrow M - k^2$. $\sigma^{xy} = \sigma^{yx} = 0$ is again due to mirror symmetries.

Supplementary Note 2. Analytic calculation of the optical conductivity in the superconducting state of a single Dirac model

Here we consider the Δ_{4a} pairing in Eq. (S1) such that the BdG Hamiltonian is

$$H = -\mu\tau_z + \hbar v k_x \tau_z \sigma_y - \hbar v k_y \sigma_x + \Delta_{4a} k_x \tau_x \sigma_x. \quad (\text{S3})$$

It has $M_x = i\sigma_x$, $M_y = i\tau_z \sigma_y$, $C_{2z} = i\tau_z \sigma_z$, $T = i\sigma_y K$, and $C = \tau_x K$ symmetries. For a simpler understanding of the analytic calculation, we perform a unitary transformation

$H \rightarrow U^{-1}HU$ using

$$U = \begin{pmatrix} 1 & 0 & 0 & 0 \\ 0 & 1 & 0 & 0 \\ 0 & 0 & 0 & 1 \\ 0 & 0 & 1 & 0 \end{pmatrix} = \frac{1}{2} (1 + \tau_z + \sigma_x - \tau_z \sigma_x) \quad (\text{S4})$$

such that the new Hamiltonian is

$$H = \hbar v (k_x \sigma_y - \hbar k_y \sigma_x) - \mu \tau_z + \Delta_{4a} k_x \tau_x. \quad (\text{S5})$$

In this form, since the σ and τ terms commute with each other, it is obvious that the energy eigenstate takes the form,

$$|\pm\rangle = |\pm\rangle_\tau \otimes |\pm\rangle_\sigma, \quad (\text{S6})$$

where $|\pm\rangle_\tau$ and $|\pm\rangle_\sigma$ are two-component states satisfying

$$\begin{aligned} (-\mu \tau_z + \Delta_{4a} k_x \tau_x) |\pm\rangle_\sigma &= \pm \sqrt{\mu^2 + (\Delta_{4a} k_x)^2} |\pm\rangle_\sigma \\ (k_x \sigma_y - k_y \sigma_x) |\pm\rangle_\tau &= \pm \sqrt{k_x^2 + k_y^2} |\pm\rangle_\tau. \end{aligned} \quad (\text{S7})$$

As σ and τ degrees are independent, the inter-band velocity matrix element between the two bands nearest to the Fermi level can be simply calculated as

$$\begin{aligned} V_{+-,-+}^a &= \frac{1}{\hbar} \langle + - | \partial_a h_0 \tau_z | - + \rangle \\ &= \frac{1}{\hbar} \langle + | \tau_z | - \rangle_\tau \langle - | \partial_a h_0 | + \rangle_\sigma \\ &= e^{i\phi} v \frac{\Delta_{4a} k_x}{\sqrt{\mu^2 + (\Delta_{4a} k_x)^2}} \frac{k_y}{\sqrt{k_x^2 + k_y^2}}. \end{aligned} \quad (\text{S8})$$

for some phase factor ϕ . For $\hbar\omega \sim \Delta_{4a} k_F \ll \mu$, where $k_F = \mu/\hbar v$, the optical conductivity is

$$\begin{aligned} \sigma^{c;c}(\omega) &= \frac{\pi e^2}{2\hbar\omega} \int_{\mathbf{k}} \sum_{n,m} f_{nm} |V_{mn}^c|^2 \delta(\omega - \omega_{mn}) \\ &\approx \frac{e^2}{\hbar} \frac{1}{\hbar\omega} \frac{(\Delta_{4a} v_F)^2}{\mu} \frac{\pi}{8} \left(1 - \frac{1}{2} \cos 2\theta_c \right) \end{aligned} \quad (\text{S9})$$

in the leading order of ω and Δ_{4a} , where $k^c = |\mathbf{k}| \cos \theta_c$, and θ_c is measured from the x axis.

Supplementary Note 3. An identity on matrix elements of the pairing Hamiltonian

Here we show that $\tau_z H_\Delta$ is a hollow matrix in the BdG energy eigenstate basis, i.e.,

$$\langle n\mathbf{k} | \tau_z H_\Delta(\mathbf{k}) | n\mathbf{k} \rangle = 0 \quad \forall n, \quad (\text{S10})$$

where $|n\mathbf{k}\rangle$ is an energy eigenstate of the BdG Hamiltonian, and

$$H_\Delta(\mathbf{k}) = \begin{pmatrix} 0 & \Delta(\mathbf{k}) \\ -\Delta^*(-\mathbf{k}) & 0 \end{pmatrix} \quad (\text{S11})$$

is the pairing part of the Hamiltonian. It can be simply shown by

$$\begin{aligned} \langle m | \tau_z H_\Delta | n \rangle &= \frac{1}{2} \langle m | [\tau_z, H_\Delta] | n \rangle \\ &= \frac{1}{2} \langle m | [\tau_z, H - H_0] | n \rangle \\ &= \frac{1}{2} \langle m | [\tau_z, H] | n \rangle \\ &= \frac{1}{2} \langle m | \tau_z | n \rangle (E_n - E_m) \\ &= 0 \text{ for } n = m, \end{aligned} \quad (\text{S12})$$

where we use that τ_z and H_Δ anti-commutes in the first line, H_0 is the normal-state Hamiltonian in the BdG form, and τ_z commutes with H_0 in the third line.

This identity can be used to understand why $\sigma^{yy} = 0$ in Fig. S1(d). Let us note that PC changes the M_z eigenvalue λ while S preserves λ for even- M_z pairing such as the Δ_5 pairing. Therefore, a potentially non-zero spectrum-inversion-symmetric excitation is due to the velocity operator between states related by the chiral operation. If we look at the y component,

$$\begin{aligned} \langle S n | V^y | n \rangle &= -\langle n | S \tau_z \rho_x \sigma_x | n \rangle \\ &= \langle n | S \rho_y \sigma_y M_z | n \rangle \\ &= \lambda_n \langle n | S \rho_y \sigma_y | n \rangle \\ &= \frac{\lambda_n}{i\Delta_5} \langle n | \tau_z H_\Delta | n \rangle, \end{aligned} \quad (\text{S13})$$

where $M_z = i\tau_z \rho_z \sigma_z$, $S = \tau_x \sigma_y$, and $H_\Delta = -\Delta_5 \tau_y \rho_y$. It is zero by the identity we derive above.